ACS OMEGA

http://pubs.acs.org/journal/acsodf

Article

CO and O_2 Adsorption and CO Oxidation on Pt Nanoparticles by Indirect Nanoplasmonic Sensing

Benjamin Demirdjian,* Igor Ozerov, Frédéric Bedu, Alain Ranguis, and Claude R. Henry

Cite This: *ACS Omega* 2021, 6, 13398−13405

Read Online

ACCESS | Metrics & More | Article Recommendations | Supporting Information

ABSTRACT: We used indirect nanoplasmonic sensing (INPS) coupled with mass spectrometry to study CO and oxygen adsorption as well as CO oxidation, on Pt nanoparticles, in the Torr pressure range. Due to an optimization of the physical parameters of our plasmonic sample, we obtain a highly sensitive probe that can detect gas adsorption of a few hundredths of a monolayer, even with a very low number density of Pt particles. Moreover and for the first time, a similarity is observed between the sign and the evolution of the localized surface plasmon resonance (LSPR) peak shift and the work function measurements for CO and oxygen chemisorption. Controlling the size, shape, and surface density of Pt particles, the turnover frequency (TOF) has also been accurately determined. For similar experimental conditions, the TOF is close to those measured on Pt/oxide powder catalysts and Pt(100) single crystals.

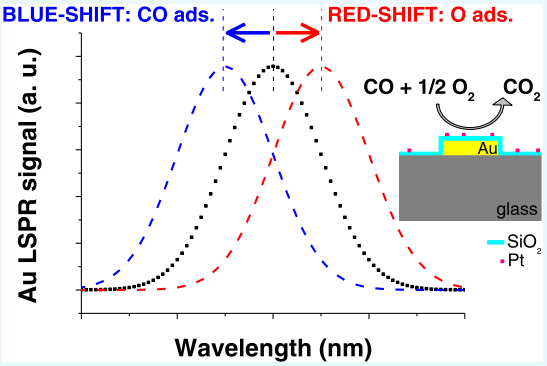

1. INTRODUCTION

Plasmons, collective oscillations of electrons in noble metals, have resonance frequencies corresponding to visible and near-infrared spectral regions for silver and gold. When gas or liquid molecules are adsorbed on nanoparticles, the minute local changes in refractive index strongly modify the optical response corresponding to localized surface plasmon resonance (LSPR) in metal nanoparticles. Consequently, the spectral position of the LSPR extinction peak, corresponding to the absorption maximum, is shifted following a simple model[1]

$$\Delta\lambda = m(n_2 - n_1)\left[1-\exp\left(\frac{-2d}{l_d}\right)\right] \quad (1)$$

where $\Delta\lambda$ is the shift in wavelength in the extinction spectra corresponding to the plasmonic resonance, when the refractive index of surrounding media changes from n_1 to n_2, and m is the refractive index sensitivity. The parameters under the exponent d and l_d correspond to the effective thickness of the adsorbed layer and the evanescent electromagnetic field decay characteristic length. l_d depends on the properties of the sensor material as well as on its geometrical characteristics.

In recent years, LSPR has been used in catalytic studies[2−8] for CO oxidation,[2,6,8] water synthesis,[2,4] and gas adsorption (CO, H_2, etc.).[3,5,7] Adsorption has been studied on Au particles or Pt nanoparticles (NPs) supported on a thin dielectric layer on Au particles. In the last case, the plasmonic technique is called indirect nanoplasmonic sensing (INPS). For catalytic reactions with Pt NPs, INPS is preferable to avoid alloying between both metals. Larsson et al.[2] have shown that the insulator layer protects and increases their stability at high temperatures. Moreover, it suppresses the electronic interactions between the Pt NPs and the Au particles. Pt NPs can react with gas molecules that change the dielectric properties at the surface of the Pt NPs and generate a shift of the LSPR wavelength of the underlying Au particle; this is an indirect LSPR phenomenon (INPS).[9]

In the studies of CO oxidation, the reaction is made on an assembly of nanoparticles with a rather large size distribution like 5−30 nm for Pt particles (Figure S1 in Larsson et al.[2]) with a more or less round shape. It has also been possible to study the reaction on a single large Pt particle (70 nm) prepared by hole mask colloidal lithography.[8] In the present paper, the shape and size of the Pt NPs are controlled in the small size range (<5 nm). Indeed, it is well known that for this catalytic reaction, the catalytic reaction rate depends on these two parameters.[10,11] In the small size domain, the nanofabrication procedure cannot be used and the classical metallic vapor deposition leads to large size dispersion unlike a template is used.[12] Thus, we turn to a wet chemical preparation method, which provides a sharp size distribution. To avoid using an organic surfactant to stabilize the particles, we modify a method described by Peng's group,[13] which was developed to grow cubic 10 nm Pt NPs. In the original

Received: March 19, 2021
Accepted: April 27, 2021
Published: May 12, 2021

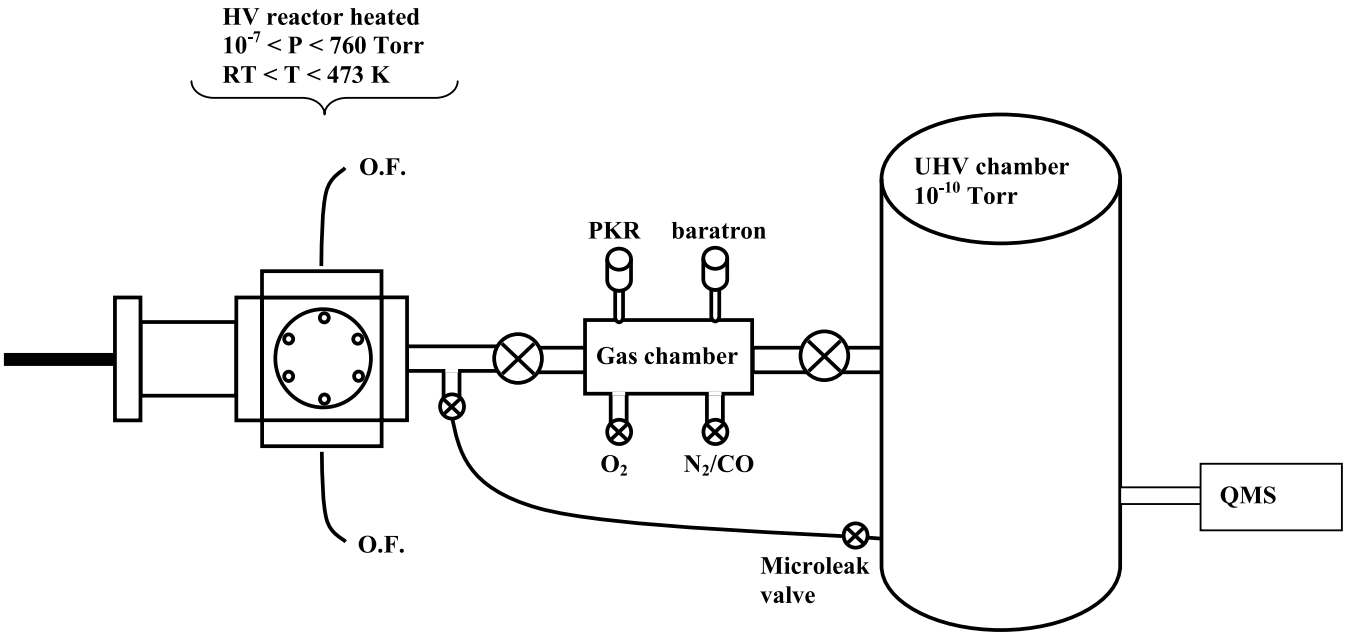

Figure 1. Schematic representation of the experimental setup for plasmonic and mass spectrometry measurements.

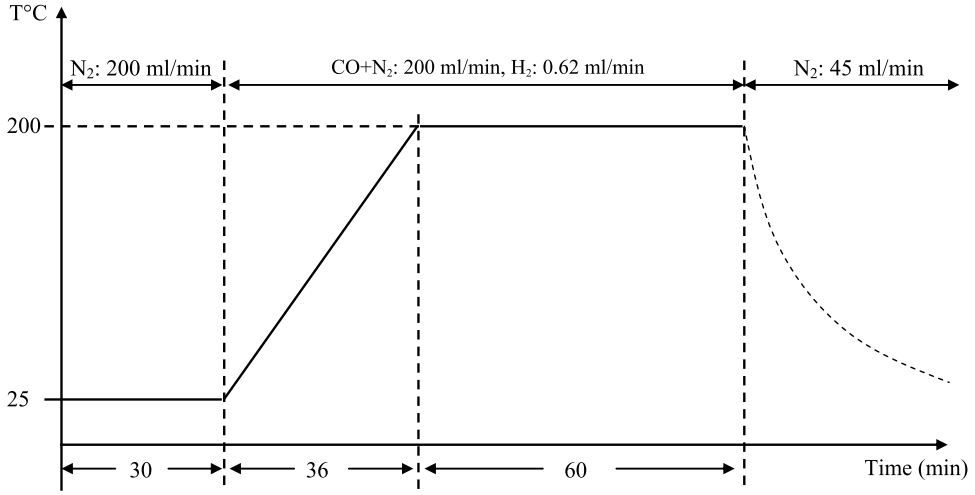

Figure 2. Heating and reduction treatment of the sample.

preparation method, a carbon powder was first impregnated by a solution of $Pt(acac)_2$ (Pt acetylacetonate) in chloroform; then, in a second step, the sample was reduced at 200 °C, under a flow of H_2 and CO. CO is known to form cubic Pt particles.[14] After 1 h reduction at 200 °C, most of the acac residues are removed.[13] To use a planar support compatible with plasmonic sensors, the original method (see Section 2.3) has been modified to obtain nanocubes with a mean size of 3 nm and narrow size distribution supported on a carbon or a SiO_2 thin film. These nanocubes were used to study by INPS the adsorption/desorption of CO and oxygen and the CO oxidation.

2. EXPERIMENTAL SECTION

2.1. Au Nanodisk Fabrication. Au nanodisk arrays are fabricated by electron beam lithography (EBL) followed by a lift-off process. The disks are supported on borosilicate glass substrates (1 in.), and experimental details can be found in refs 15, 16. This fabrication technique allows controlling the Au disk aspect ratio and their interdistances. It is crucial to optimize these parameters to have a good LSPR signal-to-noise ratio mainly for very low coverages of Pt particles. With the hole mask colloidal lithography,[2] it is impossible to continuously control all of these parameters. Our Au disks have the following parameters: interdistance, 300 nm; diameter, 150 nm; thickness, 30 nm. The plasmonic sample (Au disks/glass) is thermally annealed for 3 h at 350 °C in an oven under a He flow (250 mL/min) to stabilize the microstructure and shape of the Au nanodisks.[17] This step is important to avoid temperature-induced irreversible spectral shifts during experiments at elevated temperatures, caused by (micro)structural reshaping of the sensor particles. Typically, this thermal annealing step leads to recrystallization of the nanodisks.

2.2. Experimental Setup. The schematic representation of the experimental setup used for LSPR and quadrupole mass spectrometry (QMS) measurements is presented in Figure 1. A high vacuum (HV) reactor consists of a UHV stainless steel

https://doi.org/10.1021/acsomega.1c01487
ACS Omega 2021, 6, 13398−13405

cube (CF DN 40) with two glass windows. The sample inside the HV reactor is illuminated by an optical fiber (Avantes, IR200-FC-2) connected to a tungsten halogen source (Avantes, AvaLight-HAL-S). The fiber is mounted on a collimating lens (Avantes, COL-UV/vis), allowing to obtain a parallel light beam on the sample. The light transmitted by the sample is collected to another fiber using a similar collimator lens. The signal is collected and analyzed in the 360−900 nm spectral range by a ultraviolet−visible (UV−vis) spectrometer (CCD detector, Avantes Avaspec-ULS3648 USB2), which is monitored by the Avantes "Avasoft-Full" software. The HV reactor is heated by an external rope heater connected to a PID controller. The temperature, controlled from room temperature to 473 K, is measured inside the HV reactor with a type K thermocouple sensor.

Pure O_2 gas (purity, 99.995%; N45) and CO-containing gas mixture (CO: 9%, N_2: 91%) are used. Pressures are measured inside the gas chamber (see Figure 1) equipped with a Baratron pressure transducer (MKS type 127, 100 Torr range) and a Pirani/cold cathode transmitter (Pfeiffer Vacuum, PKR 251). To measure the gas content and the CO_2 production in the reactor, the HV reactor is connected through a leak valve to another UHV chamber equipped with a mass spectrometer (Pfeiffer Vacuum, Prisma Plus QMG 220) as shown in Figure 1.

2.3. Preparation Method of Pt Nanoparticles. To obtain a planar catalyst, different variants of the original method developed for powder supports[13] were tried: (i) drop-casting on flat support (amorphous carbon or silica thin films supported on a freshly cleaved NaCl single crystal) with different concentrations of precursor and (ii) immersion of the support in the precursor solution for a variable time and with slow stirring. After impregnation, the sample is quickly placed inside the oven and heated up to the desired reduction temperature under inert N_2 flow. Then, the gas flow is switched to a mixture of H_2 and CO for the reduction during the desired time (see Figure 2). After cooling the sample to RT, under N_2 flow, it was placed in the ambient atmosphere. The thin-film support (carbon or silica) was detached carefully from the NaCl support by interfacial dissolution in distilled water and mounted on a copper grid for subsequent transmission electron microscopy (TEM) observations (Figure 3). To finalize the best methodology giving small cubic particles with homogeneous spatial distribution and a narrow size dispersion, we used mainly the carbon films because they were more suitable for TEM observations. The optimal preparation conditions, which have been used for the preparation of the Pt catalyst for INPS experiments, are detailed in the following.

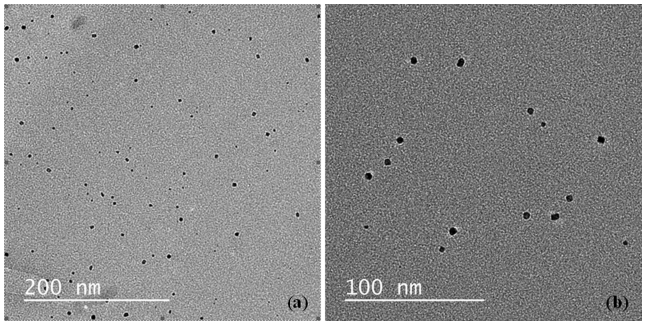

Figure 3. (a, b) TEM images of Pt NPs on carbon film at different magnifications.

The plasmonic sample (Au disks on glass support) covered by a thin film of silica (7 nm) is immersed in the solution containing 100 mg of $Pt(acac)_2$ in 15 mL of chloroform for 1 h with gentle stirring of the solution every 10 min and rapid insertion into the oven. The reduction and heating treatment is represented in Figure 2. After cooling of the sample to RT, the sample is rapidly inserted in the stainless steel HV rector for plasmonic measurement where a vacuum of 10^{-6} Torr is established.

Figure 3 shows TEM images of Pt NPs on a 10 nm carbon film that have been synthesized with the experimental conditions as those for the INPS sample. In Figure 3b, we see that most of the Pt NPs have a square outline due to the cubic shape. The density of the Pt NPs is $n_s = 5.8 \times 10^{10} \pm 0.3 \times 10^{10}$ cm^{-2}, the mean size is $d = 3.0 \pm 1$ nm, the fraction of the substrate covered by the Pt NPs is $a_s = n_s d^2 = 0.52\%$, and the area (a_e) exposed to the gases is 5 times larger (2.6%). We have also prepared Pt NPs on 10 nm silica film on NaCl under the same conditions. The characteristics of the deposit are very similar to those obtained on the carbon film.

2.4. Introduction of CO and O_2. Before the introduction of CO and O_2 gases, the HV reactor was pumped until a pressure $P \leq 10^{-6}$ Torr. We define X_{CO} as the CO molar fraction given by

$$X_{CO} = P_{CO}/(P_{CO} + P_{O_2}) \quad (2)$$

where P_{CO} and P_{O_2} are the partial pressures of CO and O_2 gases in the gas introduction ramp before the gas expansion into the HV reactor, respectively. The partial pressures in the HV reactor are monitored by a mass spectrometer in a UHV chamber (see Figure 1).

3. EXPERIMENTAL RESULTS

3.1. Oxygen Adsorption. Before studying CO oxidation, the adsorption of O_2 and CO on Pt NPs has been studied for the first time using INPS. For that purpose, we first introduced O_2 into the HV reactor at $T = 443$ K under initial pressure of 0.53 Torr and waited for 3 h. During this time, the pressure decreases due to the gas adsorption and gas effusion through the leak valve (Figure 1), from 0.53 to 0.38 Torr. In parallel, a redshift of the LSPR response was clearly observed (Figure 4). At 443 K, oxygen is irreversibly adsorbed on the Pt NPs;[18,19] then, even if the oxygen pressure in the reactor decreases, the (dissociative) adsorption increases until the saturation coverage is reached after 165 min, which corresponds to $\Delta\lambda_{max} = 0.221$ nm. From Norton the oxygen saturation coverage of oxygen is around 0.4 ML.[18]

3.2. CO Adsorption. To study CO adsorption, the gas mixture CO + N_2 (CO: 9%, N_2: 91%) was introduced into the HV reactor at $T = 443$ K at an initial pressure of 0.67 Torr. After 3 h, the total pressure decreased from 0.67 to 0.52 Torr and the CO partial pressure varied from 0.061 to 0.047 Torr. During this time, optical spectra were recorded every 15 min and they clearly showed a blueshift of the LSPR response (Figures S1 and 5). After 3 h, an LSPR shift $\Delta\lambda_{max} = -0.181$ nm is measured. At 443 K, N_2 is not adsorbed on Pt NPs and all possible traces of residual adsorbed oxygen are removed by reaction with CO, then only CO is (reversibly) adsorbed on the Pt NPs.

https://doi.org/10.1021/acsomega.1c01487
ACS Omega 2021, 6, 13398−13405

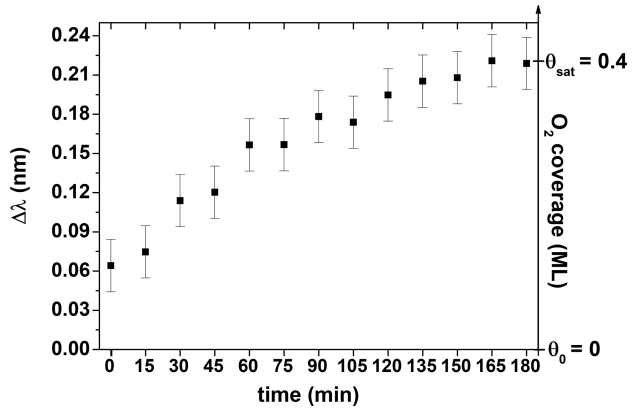

Figure 4. Experimental LSPR shifts $\Delta\lambda$ vs time at T = 443 K for Pt cubic nanoparticles deposited on Au disks covered by a silica film. The LSPR shift $\Delta\lambda$ is defined with respect to a reference, which is the plasmonic sample before oxygen adsorption. The oxygen coverage increases with time until saturation coverage. The accuracy of the wavelength measurements in the LSPR response is 0.04 nm (error bars).

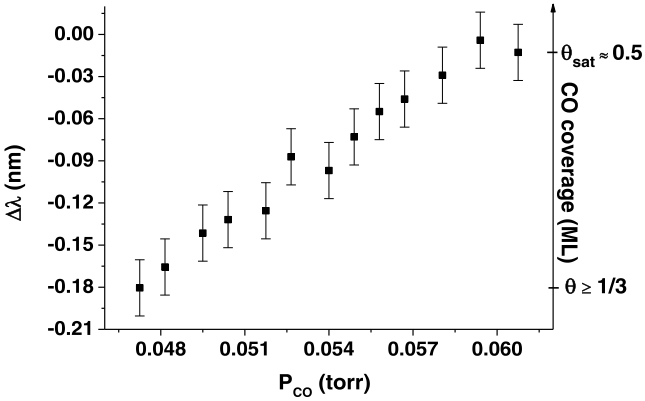

Figure 5. Experimental LSPR shifts $\Delta\lambda$ vs P_{CO} at T = 443 K for Pt cubic nanoparticles deposited on Au disks covered by a silica film. The LSPR shift is defined with respect to a reference, which is the plasmonic sample before CO adsorption. Each measurement is recorded every 15 min. The equilibrium coverage of CO increases with CO pressure. The accuracy of the wavelength measurements in the LSPR response is 0.04 nm (error bars).

In contrast to that observed for oxygen, the adsorption of CO is reversible (see the Section 4). Finally, the highest CO pressure (0.061 Torr) corresponds to the CO saturation coverage (0.5 ML) mentioned in Section 4.1[20]

3.3. CO Oxidation. *3.3.1. LSPR Measurements.* All of the CO oxidation experiments were conducted at 443 K, and the LSPR shifts $\Delta\lambda_0$ induced by the gas adsorption/reaction on the Pt particles were measured at the thermal equilibrium. The LSPR shifts $\Delta\lambda_0$ versus the ratio P_{O_2}/P_{CO} and the CO molar fraction X_{CO} are given in Table 1 and Figure 6.

In Figure 6, the experimental data show that $\Delta\lambda_0$ increases when X_{CO} decreases from 0.5 to 0.01. This observation is in agreement with the results obtained by the Langhammer's group[8] for a single Pt nanoparticle. For X_{CO} = 0.01, we measured $\Delta\lambda_0$ = 0.229 nm; for X_{CO} = 0.5, $\Delta\lambda_0$ becomes negative, i.e., $\Delta\lambda_0 = -0.171$ nm. Our previous measurements with a single gas showed that for pure oxygen, the LSPR shift $\Delta\lambda_0$ was positive and negative for pure CO gas (Table 1 and Figures 4 and 5). Thus, we conclude that at X_{CO} = 0.5, Pt is

Table 1. Different INPS Experiments vs the Ratio P_{O_2}/P_{CO} and the CO Molar Fraction X_{CO}

P_{O_2} (Torr)	P_{O_2}/P_{CO}	X_{CO} eq 1	$\Delta\lambda_0$ thermal equilibrium
0.09	1	0.5	−0.171
0.27	3	0.25	0.030
0.81	9	0.1	0.097
1.71	19	0.05	0.107
8.91	99	0.01	0.229

P_{CO} = 0.09 Torr, T = 443 K.

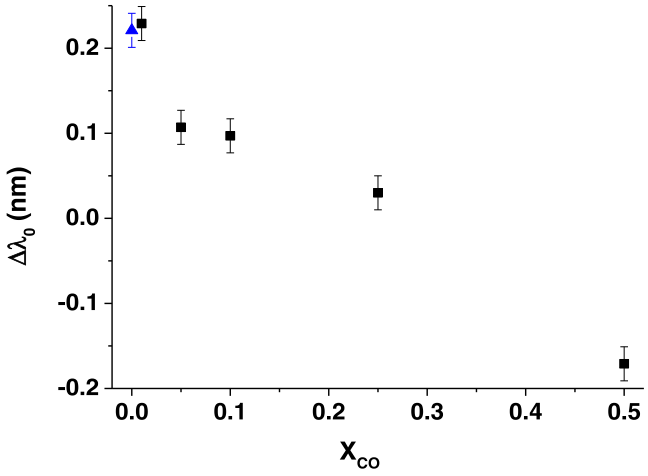

Figure 6. Experimental LSPR shifts $\Delta\lambda_0$ vs X_{CO} at T = 443 K for Pt cubic nanoparticles deposited on Au disks covered by a silica film. The LSPR shift is defined with respect to a reference, which is the plasmonic sample before gas adsorption/reaction. The blue triangle at X_{CO} = 0 corresponds to the saturation coverage in pure oxygen, i.e., $\Delta\lambda_{max}$ = 0.221 nm (see Section 3.1). The accuracy of the wavelength measurements in the LSPR response is 0.04 nm (error bars).

mainly covered by CO, and when X_{CO} decreases, the CO coverage decreases while oxygen coverage increases continuously up to almost saturation.

3.3.2. Quadrupole Mass Spectrometry (QMS) Experiments. QMS allows monitoring the production of CO_2 in the reactor. Figure 7 displays the CO_2 production during CO oxidation on the Pt NPs at T = 443 K for X_{CO} = 0.25 (P_{O_2}/P_{CO} = 3).

Figure 7c corresponds to the CO_2 production by the plasmonic sample itself since the contribution from the bare HV reactor (Figure 7a), without the plasmonic sample, has been subtracted.

If we make the difference between the ion current for mass 44 when we introduce the gas into the rector (t = 1320 s) and after 3 h (t = 12 000 s), we obtain for X_{CO} = 0.25 an ion current difference of 1.76×10^{-12} A. In Figure 8, these differences have been plotted for other values of X_{CO}, we observed that the maximum of the steady-state CO_2 production is obtained for X_{CO} = 0.05, which is in agreement with the work of Langhammer on large (70 nm) single Pt particles at 473 K.[8]

To compare the catalytic activity with previous results on supported Pt or extended surfaces, it is interesting to calculate the turnover frequency (TOF), which corresponds to the number of CO_2 molecules produced per second and per Pt surface atom. The details of the calculation are given in the Supporting Information. At 443 K, for 0.27 Torr of O_2 and

https://doi.org/10.1021/acsomega.1c01487
ACS Omega 2021, 6, 13398−13405

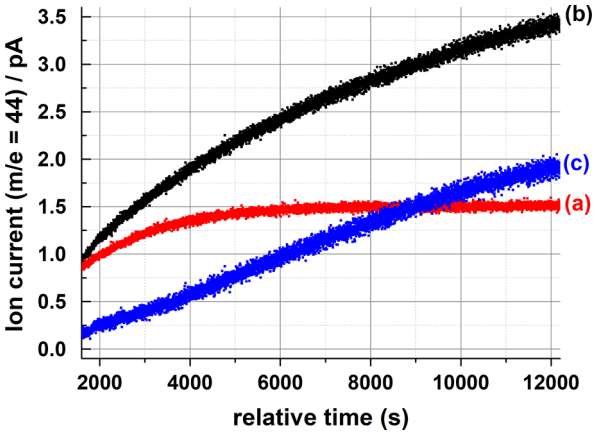

Figure 7. Ion current for m/e = 44 vs relative time for (a) the HV reactor without the plasmonic sample at T = 443 K for X_{CO} = 0.25; (b) plasmonic sample in the HV reactor at T = 443 K for X_{CO} = 0.25; and (c) difference between (b) and (a) corresponding to the real CO_2 produced by the plasmonic sample itself.

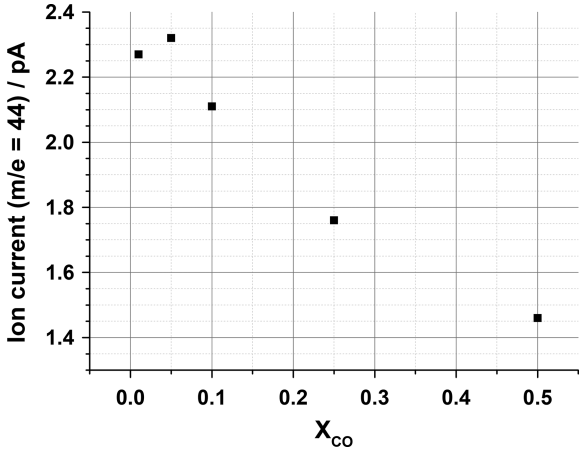

Figure 8. Ion current for m/e = 44 vs the X_{CO} molar fraction. The value of the ion current is obtained by calculating the difference between the ion current when we introduce the gas into the reactor and after 3 h; T = 443 K.

0.09 Torr of CO (X_{CO} = 0.25), the steady-state TOF is 0.07 s^{-1} that is in good agreement with literature values for Pt for similar experimental conditions (see Table 2 and the Section 4). We can also calculate under these conditions the CO-reaction probability, which is equal to 9.4 × 10^{-8}.

4. DISCUSSION

4.1. O_2 and CO Adsorption. Oxygen adsorption in the 10^{-2} Torr pressure range has been previously studied by photoelectron spectroscopy and work function measurement on polycrystalline Pt[18] and Pt(111).[19] In both cases, it was observed that the work function variation ($\Delta\Phi$) is positive and increases with oxygen coverage (Figure 9).

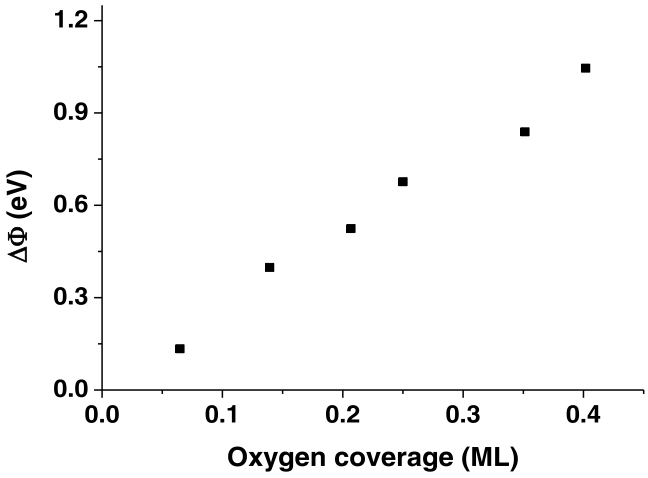

Figure 9. Evolution of the work function variation ($\Delta\Phi$) as a function of the oxygen coverage on Pt from ref18 (data from Figure 8[18] are used to plot this new graph).

The saturation coverage at RT on polycrystalline Pt is around 0.4 ML.[18] Assuming the same value for the saturation coverage on our Pt particles, one can estimate from the accuracy of the $\Delta\lambda$ measurements that the minimum coverage detectable with the INPS method is about 0.04 ML (see error bars in Figure 4). However, by increasing the exposed area of Pt up to 40%, the sensitivity would be 1.6 × 10^{-3} ML.

CO adsorption has also been studied with the same techniques at low pressures (10^{-7}−10^{-5} Torr) on Pt(111)[19,20] and Pt(100).[21] Contrary to the oxygen case upon CO adsorption on Pt(111), the variation of the work function is negative. At low coverage, $\Delta\Phi$ decreases up to a coverage of 1/3 ML; then, it increases up to saturation coverage of 1/2 ML (Figure 10). It is interesting to note that at zero coverage and saturation $\Delta\Phi$ tends to a value close to zero.

On Pt(100), the situation is more complicated because the Pt surface is reconstructed to a quasi-hexagonal structure, but the variation of $\Delta\Phi$ on the reconstructed surface is similar to Pt(111).[21] CO adsorption on 4 nm Pt particles supported on Al_2O_3 has been studied by infrared spectroscopy.[22] This work

Table 2. TOF and CO-Reaction Probability Measured in the Present Study and in Published Works under Similar Experimental Conditions for Supported Pt Particles of Different Sizes (d) and Pt(100)

TOF (s^{-1})	reaction probability	T (K)	P_{O_2} (Torr)	P_{CO} (Torr)	P_{O_2}/P_{CO}	system	d (nm)	reference
0.07	9.4 × 10^{-8}	443	0.27	0.09	3	Pt cubes/SiO_2	3	present study
0.04		450	4.5	9.7	0.46	Pt/SiO_2	4[a]	29
	5 × 10^{-8}/3 × 10^{-7}	460	38	12.7	3	Pt/Al_2O_3	4	30
0.03		443	2.7	5.3	0.5	Pt/SiO_2	2.6−4.2	31
0.005[b]		443	7.6	7.6	1	Pt cubes/Al_2O_3	8	32
0.03/0.04		443	8	16	0.5	Pt(100)		33

[a]The particle size is tentatively calculated from the dispersion (D = 0.22) in Cant et al.[29] following the formula d (nm) = 0.9/D. [b]The TOF value is derived from the rate of CO_2 molecules produced by gram and per second taking the cubic shape and the size of the Pt particles.[32]

https://doi.org/10.1021/acsomega.1c01487
ACS Omega 2021, 6, 13398−13405

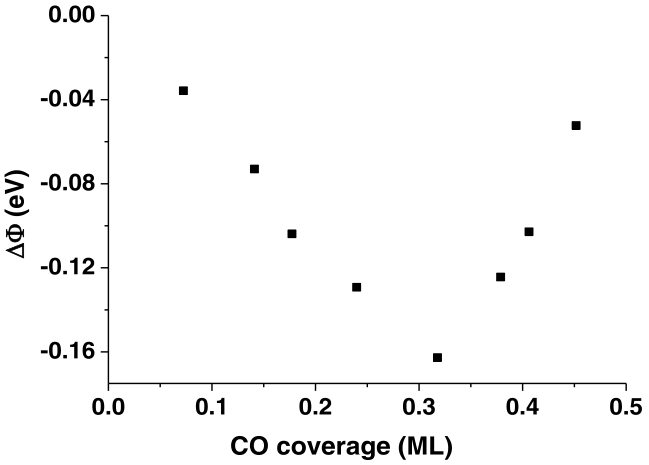

Figure 10. Evolution of the work function variation ($\Delta\Phi$) as a function of CO coverage on Pt from ref20 (data from Figure 7[20] are used to plot this new graph).

shows that at 460 K, the saturation coverage is not reached under 75 Torr of CO and that at 520 K, CO adsorption is completely reversible. Ertl's group[20,23] has shown that the adsorption energy of CO strongly decreases with coverage from 30 kcal/mol at zero coverage to 22 kcal/mol at a coverage of 0.5 ML; then, at this coverage, the lifetime of a CO molecule would be 7×10^{-6} s. Recent DFT calculations[24] have shown that under the conditions of the present experiment (T = 443 K and 0.05 < P_{CO} < 0.06 Torr), the equilibrium CO coverage is in the range 0.33−0.5 ML for Pt(111) and 0.67−0.75 ML for Pt(100). Then, the CO coverage is always larger than 1/3 ML, which means that $\Delta\Phi$ is increasing with CO coverage (see Figure 10).[19−21] It is striking that in the INPS experiments, the sign of $\Delta\lambda$ is reversed from oxygen to CO adsorption like for $\Delta\Phi$ measurements. Moreover, $\Delta\Phi$ and $\Delta\lambda$ increase with CO coverage. It is beyond our scope to go deep into the explanation of this analogy between work function and plasmon shift, but it is reasonable to recall that both measurements depend on the variation of the dipole moment and the organization of the CO molecules in the adsorbed layer. Indeed, the work function is, from Lang and Kohn's model,[25] equal to the difference between the dipole layer contribution (D) and the internal chemical potential (μ). In the case of a chemisorbed layer, the variation of μ is negligible, then $\Delta\Phi \approx \Delta D$. Following this idea, Norton[18] and Ertl[20] explain the variation of $\Delta\Phi$ with oxygen and CO coverage by the variation of the dipole moment of the adsorbed layer that depends on the coverage and of the organization of adsorbed molecules. In LSPR experiments (used to follow gas adsorption), the variation of $\Delta\lambda$ has been attributed to either a change of the electron density in the Au particles due to charge transfer or a change in the dielectric constant (ε) of the matrix around the Au particles.[5] In the case of CO adsorption on Au-YSZ (yttria-stabilized zirconia) composite, charge transfer toward Au particles has been invoked[26] while for CO adsorption in the Au−CuO system, the change in the dielectric function of the matrix was put forward.[27] However, in INPS, it has been shown that charge transfer toward the Au nanoparticles is negligible due to the thin SiO_2 film.[28] Therefore, we believe that in our case, the shift of the Au plasmon peak is mainly due to the change of the dielectric constant of the matrix around the Au particles. The modification of the polarization of the Pt particles by the dipole layer formed by the adsorbate would be responsible for the change of ε.

4.2. CO Oxidation. Several studies have reported TOF measurements on Pt NPs, under experimental conditions close to those used in the present study.[29−32] These data are reported in Table 2 with the present measurements, and for comparison, the results on Pt(100).[33]

From Table 2, we can see that for supported Pt NPs (diameter, 3−8 nm) at 443 K and pressures in the range of 10^{-1}−10^{2} Torr, the measured TOFs are in the range of 0.03−0.04 s^{-1}, which is rather close to the present measurement (0.07 s^{-1}). In the case of 8 nm Pt cubes[32] prepared by a colloidal method, the measured TOF is smaller that could be due to the remaining ligands on the surface of the Pt particles. In the present measurement, no ligand was present in the preparation method. In one case,[30] the TOF is not given in the publication but the value of the CO-reaction probability (5×10^{-8}−3×10^{-7}) is close to the value obtained in this study (9.4×10^{-8}). The present results are also close to the TOF measured on Pt(100) by Goodman's group[33] at 443 K. As the size of the Pt particles in the different studies varies between 3 and 8 nm in Table 2, one could expect a size effect in the reaction rate, but in all cases, we are in the CO-rich regime for which the reaction is structure insensitive.[31,32] However, the maximum of CO_2 production is obtained for P_{O_2}/P_{CO} = 19 (or X_{CO} = 0.05, Table 1), which clearly corresponds to the O-rich regime.

The variation of the Au LSPR peak shift ($\Delta\lambda_0$) as a function of X_{CO} (Figure 6) expresses the transition from an O-rich regime to a CO-rich regime when X_{CO} increases as it has been previously observed by Langhammer.[2,8] However, the shift in plasmonic absorption spectra they observed was much larger than that we obtained in the present study. For example, the shift for X_{CO} = 0, corresponding to the saturation oxygen coverage, appears around 1 nm in the former study while it is around 0.2 nm in the present study. This smaller value is due to the much weaker coverage of Pt NPs in the present study. The Pt-exposed area in the present study (2.6%) is 15 times smaller than in the Langhammer's study (40% in this case).[2] Then, we can expect that sensitivity in the present study increases by a factor of 15. This increase in sensitivity of the INPS technique is probably due to a better regularity of the underlying plasmonic gold particles, which are prepared by e-beam lithography that allows an optimization of the aspect ratio of the Au disks and their separation distance.[15,16] Finally, it would be interesting to improve INPS by simply monitoring the light intensity on the steepest part of the absorption peak. The change in intensity would be proportional to the shift in resonance wavelength.[34] One could get the same signal-to-noise ratio (S/N) in LSPR orders of magnitude faster that way.

5. CONCLUSIONS

In this study, we show that indirect nanoplasmonic sensing coupled with mass spectrometry is a very efficient method to study CO and oxygen adsorption as well as CO oxidation in the 0.1−10 Torr pressure range. Our planar model catalyst is constituted by Pt nanocubes supported on a thin silica film covering a regular array of Au disks fabricated by EBL on a glass substrate. The oxygen and CO chemisorption show an increase of $\Delta\lambda$ with coverage but an opposite sign ($\Delta\lambda$ is negative in the case of CO adsorption). This behavior is similar to work function measurements. During CO oxidation, the

https://doi.org/10.1021/acsomega.1c01487
ACS Omega 2021, 6, 13398−13405

measurement of $\Delta\lambda$ with an increasing molar fraction of CO shows a transition between an O-rich regime and a CO-rich regime. CO_2 formation, measured by mass spectrometry, is maximal in the O-rich regime. The TOF has been accurately determined knowing the size, shape, and surface density of Pt particles. For similar experimental conditions, the TOF is close to those measured on Pt/oxide powder catalysts and Pt(100) single crystals. The sensitivity of the INPS technique for application in catalysis is very high since it allows following chemisorption and catalytic reaction on nanoparticles covering only 0.5% of the surface of the planar support. Moreover, the LSPR technique can be used for all gas pressures from UHV to ambient atmosphere.

■ ASSOCIATED CONTENT

Supporting Information

The Supporting Information is available free of charge at https://pubs.acs.org/doi/10.1021/acsomega.1c01487.

Calculation of the turnover frequency (TOF) and the CO-reaction probability (RP) (Figure S1) (PDF)

■ AUTHOR INFORMATION

Corresponding Author

Benjamin Demirdjian − *Aix Marseille Univ, CNRS, CINAM, Marseille, France;* orcid.org/0000-0003-1453-5041; Phone: +33 (0)6 6036 2818; Email: demirdjian@cinam.univ-mrs.fr; Fax: +33 (0)4 9141 8916

Authors

Igor Ozerov − *Aix Marseille Univ, CNRS, CINAM, Marseille, France;* orcid.org/0000-0001-5839-7854

Frédéric Bedu − *Aix Marseille Univ, CNRS, CINAM, Marseille, France*

Alain Ranguis − *Aix Marseille Univ, CNRS, CINAM, Marseille, France*

Claude R. Henry − *Aix Marseille Univ, CNRS, CINAM, Marseille, France;* orcid.org/0000-0002-7600-7239

Complete contact information is available at: https://pubs.acs.org/10.1021/acsomega.1c01487

Notes

The authors declare no competing financial interest.

■ ACKNOWLEDGMENTS

Nanofabrication processes were performed in PLANETE cleanroom facility (CINaM, Marseille). The authors sincerely thank the laboratory electron microscopy service and its agents (A. Altie and D. Chaudanson) for assisting us in TEM observations.

■ REFERENCES

(1) Jung, L. S.; Campbell, C. T.; Chinowsky, T. M.; Mar, M. N.; Yee, S. S. Quantitative interpretation of the response of surface plasmon resonance sensors to adsorbed films. *Langmuir* **1998**, *14*, 5636−5648.

(2) Larsson, E. M.; Langhammer, C.; Zoric, I.; Kasemo, B. Nanoplasmonic probes of catalytic reactions. *Science* **2009**, *326*, 1091−1094.

(3) Dharmalingam, G.; Joy, N. A.; Grisafe, B.; Carpenter, M. A. Plasmonics-based detection of H_2 and CO: discrimination between reducing gases facilitated by material control. *Beilstein J. Nanotechnol.* **2012**, *3*, 712−721.

(4) Wettergren, K.; Hellman, A.; Cavalca, F.; Zhdanov, V. P.; Langhammer, C. Unraveling the Dependence of Hydrogen Oxidation Kinetics on the Size of Pt Nanoparticles by in operando Nanoplasmonic Temperature Sensing. *Nano Lett.* **2015**, *15*, 574−580.

(5) Collins, S. S. E.; Cittadini, M.; Pecharroman, C.; Martucci, A.; Mulvaney, P. Hydrogen spillover between single Au nanorods and metal oxide supports: a surface plasmon spectroscopy study. *ACS Nano* **2015**, *9*, 7846−7856.

(6) Bu, Y.; Niemantsverdriet, J. W.; Fredriksson, H. O. A. Cu Model Catalyst Dynamics and CO Oxidation Kinetics Studied by Simultaneous in Situ UV−Vis and Mass Spectroscopy. *ACS Catal.* **2016**, *6*, 2867−2876.

(7) Watkins, W. L.; Borensztein, Y. Mechanism of hydrogen adsorption on gold nanoparticles and charge transfer probed by anisotropic surface plasmon resonance. *Phys. Chem. Chem. Phys.* **2017**, *19*, 27397−27405.

(8) Liu, S.; Arce, A. S.; Nilsson, S.; Albinson, D.; Hellberg, L.; Alekseeva, S.; Langhammer, C. In Situ Plasmonic Nanospectroscopy of the CO Oxidation Reaction over Single Pt Nanoparticles. *ACS Nano* **2019**, *13*, 6090−6100.

(9) Langhammer, C.; Larsson, E. M. Nanoplasmonic In Situ Spectroscopy for Catalysis Applications. *ACS Catal.* **2012**, *2*, 2036−2045.

(10) Henry, C. R. Surface studies of supported model catalysts. *Surf. Sci. Rep.* **1998**, *31*, 231−325.

(11) Roldan Cuenya, B.; Behafarid, F. Nanocatalysis: size-and shape-dependent chemisorption and catalytic reactivity. *Surf. Sci. Rep.* **2015**, *70*, 135−187.

(12) Henry, C. R. 2D-Arrays of Nanoparticles as Model Catalysts. *Catal. Lett.* **2015**, *145*, 731−749.

(13) Zhang, C.; Norooz, S.; Hwang, S. Y.; Kong, X.; Peng, Z. A Generic Wet Impregnation Method for Preparing Substrate-Supported Platinum Group Metal and Alloy Nanoparticles with Controlled Particle Morphology. *Nano Lett.* **2016**, *16*, 164−169.

(14) Kang, Y.; Xie, X.; Murray, C. B. Size- and Shape-Selective Synthesis of Metal Nanocrystals and Nanowires Using CO as a Reducing Agent. *Angew. Chem. Int. Ed.* **2010**, *49*, 6156−6159.

(15) Demirdjian, B.; Bedu, F.; Ranguis, A.; Ozerov, I.; Henry, C. R. Water Adsorption by a Sensitive Calibrated Gold Plasmonic Nanosensor. *Langmuir* **2018**, *34*, 5381−5385.

(16) Demirdjian, B.; Bedu, F.; Ranguis, A.; Ozerov, I.; Karapetyan, A.; Henry, C. R. Indirect Nanoplasmonic Sensing to Probe with a High Sensitivity the Interaction of Water Vapor with Soot Aerosols. *J. Phys. Chem. Lett.* **2015**, *6*, 4148−4152.

(17) Langhammer, C.; Larsson, E. M.; Kasemo, B.; Zoric, I. Indirect Nanoplasmonic Sensing: Ultrasensitive Experimental Platform for Nanomaterials Science and Optical Nanocalorimetry. *Nano Lett.* **2010**, *10*, 3529−3538.

(18) Norton, P. R. An investigation of the adsorption of oxygen and oxygen containing species on Pt by photoelectron spectroscopy. *Surf. Sci.* **1975**, *47*, 98−114.

(19) Collins, D. M.; Spicer, W. E. The adsorption of CO, O_2 and H_2 on Pt. II Ultraviolet photoelectron spectroscopy studies. *Surf. Sci.* **1977**, *69*, 114−132.

(20) Ertl, G.; Neumann, M.; Streit, K. M. Chemisorption of CO on the Pt(111) surface. *Surf. Sci.* **1977**, *64*, 393−410.

(21) Behm, R. J.; Thiel, P. A.; Norton, P. R.; Ertl, G. The interaction of CO on Pt(100). I. Mechanism of adsorption and Pt phase transition. *J. Chem. Phys.* **1983**, *78*, 7437−7447.

(22) Haaland, D. M. Infrared studies of CO adsorbed on Pt/Al_2O_3: Evidence of CO bonded in 3-fold coordination. *Surf. Sci.* **1987**, *185*, 1−14.

(23) Thiel, P. A.; Behm, R. J.; Norton, P. R.; Ertl, G. The interaction of CO on Pt(100). II. Energetic and kinetic parameters. *J. Chem. Phys.* **1983**, *78*, 7448−7458.

(24) Sumaria, V.; Nguyen, L.; Tao, F. F.; Sautet, P. Optimal packing of CO on Pt(100) and Pt(111) surfaces. *ACS Catal.* **2020**, *10*, 9533−9544.

(25) Lang, N. D.; Kohn, W. Theory of Metal Surfaces: Work Function. *Phys. Rev. B* **1971**, *3*, 1215−1223.

(26) Sirinakis, G.; Siddique, R.; Manning, I.; Rogers, P. H.; Carpenter, M. A. Development of Au-YSZ surface plasmon resonance based sensing materials: High temperature detection of CO. *J. Phys. Chem. B* **2006**, *110*, 13508−13511.
(27) Ando, M.; Kobayashi, T.; Iijima, S.; Haruta, M. Optical sensitivity of Au-CuO composite film by use of the plasmon absorption change. *Sens. Actuators, B* **2003**, *96*, 589−595.
(28) Zhdanov, V. P.; Langhammer, C. Charge transfer between sensing and targeted metal nanoparticles in indirect nanoplasmonic sensors. *Phys. E* **2017**, *87*, 205−208.
(29) Cant, N. W.; Hicks, P. C.; Lennon, B. S. Steady state oxidation of carbon monoxide over supported noble metals with particular reference to platinum. *J. Catal.* **1978**, *54*, 372−383.
(30) Haaland, D. M.; Williams, F. L. Simultaneous measurement of CO oxidation rate and surface coverage on Pt/Al_2O_3 using infrared spectroscopy: Rate hysteresis and CO island formation. *J. Catal.* **1982**, *76*, 450−465.
(31) McClure, S. M.; Lundwall, M.; Zhou, Z.; Yang, F.; Goodman, D. W. Characterization of Pt/SiO2 model catalyst at UHV and near atmospheric pressures. *Catal. Lett.* **2009**, *133*, 298−306.
(32) Kang, Y.; Li, M.; Cai, Y.; Cargnello, M.; Diaz, R. E.; Gordon, T. R.; Wieder, N. L.; Adzic, R. R.; Gorte, R. J.; Stach, E. A.; Murray, C. B. Heterogeneous catalysts need not to be so "heterogeneous": Monodisperse Pt Nanocrystals by combining shape-controlled synthesis and purification by colloidal recrystallization. *J. Am. Chem. Soc.* **2013**, *135*, 2741−2747.
(33) Berlowitz, P. J.; Peden, C. H. F.; Goodman, D. W. Kinetics of CO oxidation on single-crystal Pd, Pt, and Ir. *J. Phys. Chem. A* **1988**, *92*, 5213−5221.
(34) Shumaker-Parry, J. S.; Campbell, C. T. Quantitative Methods for Spatially Resolved Adsorption/Desorption Measurements in Real Time by Surface Plasmon Resonance Microscopy. *Anal. Chem.* **2004**, *76*, 907−917.

https://doi.org/10.1021/acsomega.1c01487
ACS Omega 2021, 6, 13398−13405